RSC Advances

PAPER

View Article Online
View Journal | View Issue

Open Access Article. Published on 28 April 2023. Downloaded on 11/13/2025 1:50:14 PM.
This article is licensed under a Creative Commons Attribution-NonCommercial 3.0 Unported Licence.

Check for updates

Cite this: *RSC Adv.*, 2023, **13**, 13195

Polymeric copper(II) and dimeric oxovanadium(V) complexes of amide–imine conjugate: bilirubin recognition and green catalysis†

Jayanta Das,[a] Sabyasachi Ta,[a] Noor Salam,[ab] Sudipta Das,[c] Subhasis Ghosh[a] and Debasis Das *[a]

An exceptionally simple amide–imine conjugate, (*E*)-*N*′-(4-(diethylamino)-2-hydroxybenzylidene)-4-methylbenzohydrazide (**L**), derived by the condensation of 4-methyl-benzoic acid hydrazide (**PTA**) with 4-(diethylamino)-2-hydroxybenzaldehyde was utilized to prepare a dimeric oxo-vanadium (**V1**) and a one-dimensional (1D) copper(II) coordination polymer (**C1**). The structures of **L**, **V1** and **C1** were confirmed by single crystal X-ray diffraction analysis. The experimental results indicate that **V1** is a promising green catalyst for the oxidation of sulfide, whereas **C1** has potential for a C–S cross-coupling reaction in a greener way. Most importantly, **C1** is an efficient 'turn-on' fluorescence sensor for bilirubin that functions *via* a ligand displacement approach. The displacement equilibrium constant is 7.78×10^5 M^{-1}. The detection limit for bilirubin is 1.15 nM in aqueous chloroform (chloroform/water, 1/4, v/v, PBS buffer, and pH 8.0).

Received 1st February 2023
Accepted 13th April 2023

DOI: 10.1039/d3ra00702b

rsc.li/rsc-advances

Introduction

The significance of amide functionality has attracted special attention in pharmaceutical chemistry[1,2] as reflected by the fact that ∼25% of drug molecules contain amide functionalities.[3] Moreover, conformational diversities allow amide moieties to be useful in synthetic chemistry.[4–10] However, metal complexes having variable oxidation states are promising catalysts for organic transformation and the synthesis of bio-active compounds and functional materials.

In this context, oxo-vanadium(V) complexes play a vibrant role in several biochemical processes, such as insulin mimicking activities,[11–13] anti-cancer activities,[14–17] nitrogen fixation,[18] halo peroxidation,[19] phosphorylation[20] and sulphide oxidation.[21] Sulphide oxidation plays a crucial role in the activation of enzymes and useful synthetic intermediates in several chemical and bio-active molecules.[22–24] Traditional synthesis generates a significant amount of waste[25–27] and causes over-oxidation, leading to sulfones.[28] To overcome the issues regarding selectivity and yield, metal complexes may play a significant role as catalysts.[29–35]

However, Cu(II) complexes have occasionally been employed as catalyst, antiviral, antibacterial and anti-tumor agents.[36–43] Several Cu(II) complexes have also been used for trace level detection and estimation of amino acids.[37–40] Most notably, copper-catalyzed Ullmann-type C–S cross coupling reaction is very useful.[44] Aryl sulphide component is commonly encountered in several drugs for the treatment of diseases, such as Alzheimer's, Parkinsons, cancer, HIV, diabetes and inflammation.[45] The transition metal complex catalyzed C–S cross-coupling reactions have been relatively less explored compared to other carbon–heteroatom bonds, *viz.* C–N, C–O and C–P, probably owing to the associated S–S coupling and poisoning of the catalyst, particularly thiophilic Pd-based catalysts.[46] To overcome catalyst poisoning, different systems, such as palladium compounds,[47–50] nickel compounds,[51,52] CoI_2(-dppe)/Zn,[53] $In(OTf)_3$,[54] $FeCl_3$ (ref. 55 and 56) and copper compounds,[57–63] have been employed. However, it requires unfavourable reaction conditions, such as toxic polar solvent, high temperature (over 200 °C) and high catalyst loading.[64] Hence, there is ample scope to contribute to the development of environment-/reaction-friendly and efficient catalysts for Ullmann-type C–S cross coupling reactions.

In addition, the literature suggests that metal complexes are potential candidates for the recognition of bio-molecules[65–68] and bio-relevant analytes.[69–73] Bilirubin ($C_{33}H_{36}N_4O_6$), a natural yellow colored linear tetrapyrrole compound, is catabolically produced by the degradation of red blood cells (RBCs) in the body.[74,75] After its formation in the tissue, heme is transported

[a]Department of Chemistry, The University of Burdwan, Burdwan 713104, WB, India. E-mail: ddas100in@yahoo.com; Fax: +91-342-2530452; Tel: +91-342-2533913, ext. 424

[b]Department of Chemistry, Surendranath College, 24/2 MG Road, Kolkata 700009, WB, India

[c]Raina Swami Bholananda Vidyayatan, Burdwan 713421, WB, India

† Electronic supplementary information (ESI) available: NMR, Mass, FTIR, UV-vis, fluorescence spectra. CCDC 1837654, 1837659 and 1837665. For ESI and crystallographic data in CIF or other electronic format see DOI: https://doi.org/10.1039/d3ra00702b

© 2023 The Author(s). Published by the Royal Society of Chemistry

Open Access Article. Published on 28 April 2023. Downloaded on 11/13/2025 1:50:14 PM. This article is licensed under a Creative Commons Attribution-NonCommercial 3.0 Unported Licence.

to the liver in an unconjugated form using serum albumin as a carrier protein. In the liver, bilirubin predominantly transforms into bilirubin diglucuronide *via* an enzymatic conjugation reaction. This conjugated bilirubin, unlike unconjugated bilirubin, is fairly water soluble and thus excreted *via* the bile.[76,77] The normal bilirubin concentration in the blood of a healthy and adult person lies in the range of 0.3–1.9 mg dL^{-1}, including conjugated bilirubin (CB) (0.1–0.4 mg dL^{-1}), unconjugated bilirubin (UCB or free bilirubin) (0.2–0.7 mg dL^{-1}) and a trace amount of non-protein-bound unconjugated bilirubin.[78,79] It is already known that bilirubin level in new born babies is almost ten times higher than that of adults.[80] A low level of serum bilirubin concentration is associated with several clinical symptoms *viz.* iron deficiency and coronary artery disease, whereas its higher concentration (>2.5 mg dL^{-1}) leads to hyper-bilirubinemia or jaundice. The elevated level of serum bilirubin in new-born babies often causes neonatal jaundice with symptoms of yellow skin and sclera, liver diseases (*viz.* cirrhosis and hepatitis), hearing loss, athetosis, brain damage related to lifelong neurologic sequelae (kernicterus) or even death.[81,82]

Although several methods of bilirubin determination, such as Jendrassik–Grofmethod, spectrophotometric method,[83,84] HPLC,[85,86] chemiluminescence combined with flow injection analysis,[87,88] capillary micellar electrokinetic chromatography[89,90] and bilirubin oxidase enzymatic analysis are available,[91,92] fluorescence technique has more advantage over others owing to its operational simplicity, instantaneous response, high sensitivity, and non-destructive methodology.[93–95] Hence, the development of fluorescence-based bilirubin sensors has attracted immense attention. For example, recognition of unconjugated, conjugated and total bilirubin has been performed using a D-glucuronic acid appended polymer (PF-Ph-GlcA),[96] modified MOF (UIO-66-PSM),[97] Zr-MOF: Eu^{3+} probe,[98] HSA-AuNCs,[99] L-cysteine modulated-CuNCs,[100] BSA-CuNCs,[101] Fe(III)-modulated BSA-CuNCs,[102] 2,2′-((1*E*,1′*E*)-(6-bromopyridine-2,3-diyl) bis-(azanylylidene)) bis-(methanylylidenediphenol),[103] fiber optic fluorescent biosensors,[80,104] $Ru(bipy)_3^{2+}$,[105] S,N-doped CDs[106] and 4,4,4-trifluoro-1-(thiophen-2-yl)-butane-1,3-dione europium(III) complex ($Eu(tta)_3$),[107] pyrene based Schiff-base,[108] polystyrene based probe,[109] and N-doped graphene QDs/$CoFe_2O_4$-DOPA/H_2O_2 system.[110]

A careful review of the literature indicates that very few metal complex-based bilirubin sensors[111,112] are available that function *via* a fluorescence quenching mechanism, a highly undesirable protocol. Herein, we explored a 1D copper(II) coordination polymer (**C1**) for the recognition of bilirubin *via* "turn-on fluorescence" without any significant interference from competing bio-molecules. We proposed that the recognition of bilirubin proceeds *via* the "ligand displacement approach"[113,114] in which the amide–imine conjugate (**L**) from the **C1** is displaced by bilirubin in solution, resulting in the fluorescence enhancement of the system. Moreover, it is found that the dimeric oxovanadium(V) (**V1**) and 1D copper(II) coordination polymer (**C1**) of the amide–imine conjugate efficiently catalyse the oxidation of sulphide and C–S cross-coupling reactions in a greener way, respectively.

Experimental

Synthesis

4-Methyl-benzoic acid hydrazide (PTA, Scheme 1). 4-Methyl-benzoic acid hydrazide (**PTA**) was synthesized by the developed procedure.[115] Calculated yield: 76%. Anal. calcd (%) for $C_8H_{10}N_2O$: C, 73.98; H, 6.71 and N, 18.65; found: C, 73.65; H, 6.82 and N, 18.71. ESI-MS (p^+) spectrum shows *m*/*z* at 151.602 and 173.659 for [**PTA** + H^+] and [**PTA** + Na^+] adduct (Fig. S1, ESI†). ^{1}H NMR (Fig. S2, ESI†) [400 MHz, DMSO-d_6, TMS, *J* (Hz), *δ* (ppm)]: (a) 9.698 (1H, s), (b) 3.557 (2H, s), (c) 2.320 (3H, s), aromatic proton. 7.695 (2H, d, $J = 8$) and 7.23 (2H, d, $J = 8$). ^{13}C NMR (Fig. S3, ESI†): 166.24, 141.27, 130.57, 129.11, 127.15, 21.14. FTIR spectrum (Fig. S4, ESI†) (KBr, cm^{-1}): 2821 *ν*(C–H aromatic); 2970 *ν*(N–H); 1657 *ν*(C=O) and 1271 *ν*(N–N).

(*E*)-*N*′-(4-(Diethylamino)-2-hydroxybenzylidene)-4-methylbenzohydrazide (L, Scheme 1). A mixture of 4-methylbenzoic acid hydrazide (**PTA**) (150 mg, ∼1 mmol) and 4-(diethylamino)-2-hydroxybenzaldehyde (193 mg, ∼1 mmol) in methanol is refluxed for 6 hours, and the resulting brown solution was kept for slow evaporation. After three days, X-ray quality needle-shaped brown crystals were isolated at 82% yield. X-ray crystallographic analysis is performed using a Bruker SMART APEXIII CCD diffractometer with Mo-Kα radiation ($\lambda = 0.71073$ Å). **L** belongs to the '$P\bar{1}$' space group. The crystallographic refinement parameters are listed in Table S1, ESI.† Anal. calcd (%) for $C_{19}H_{23}N_3O_2$: C, 70.13; H, 7.12 and N, 12.91; found: C, 71.01; H, 7.27 and N, 12.87. ^{1}H NMR (Fig. S5, ESI†) [400 MHz, $CDCl_3$, TMS, *J* (Hz), *δ*(ppm)]: (a) 11.792 (1H, s, –CONH), (b) 11.506 (1H, s, –OH), (c) 8.410 (1H, s, –N–CH–), (d) 2.372 (3H, s, $-CH_3$), (e) 3.369 (4H, m), (f) 1.09 (6H, t, $J = 7.2$), 7.815 (2H, d, $J = 8$), 7.326 (2H, d, $J = 8$), 7.178 (1H, d, $J = 8.8$), 6.116 (1H, d, $J = 2.4$) and 6.116 (1H, d, $J = 2.4$).^{13}C NMR (Fig. S6, ESI†): 162.55, 160.17, 150.56, 150.24, 142.19, 132.09, 130.71, 129.50, 127.95, 106.91, 104.08, 97.94, 44.26, 21.50 and 13.00. ESI-MS (p^+) (Fig. S7, ESI†) *m*/*z* calculated. For $C_{19}H_{23}N_3O_2$: 325.18, found: 326.48 (100%). FTIR (KBr, cm^{-1}) (Fig. S8, ESI†), 3279 *ν*(N–H); 1595 *ν*(C=N); 1632 *ν*(C=O); 3029 *ν*(C–H); 1279 *ν*(N–N). The quantum yield is 0.78.

Dinuclear oxovanadium(V) complex (V1). A mixture of methanol solutions of $VOSO_4$ (0.033 g, 1 mmol, and 5 mL) and **L** (0.065 g and 1 mmol) was stirred for 4 hours at room temperature (Scheme 2). The slow evaporation of the solvent resulted in dark brown crystals, which are suitable for X-ray diffraction analysis. Calcd yield, 73%. Single crystal X-ray diffraction analysis was performed using a Bruker SMART APEXIII CCD diffractometer with Mo-Kα radiation ($\lambda = 0.71073$ Å), confirming the structure of the **V1**. It belongs to the '$P\bar{1}$' space group. The crystallographic refinement parameters are listed in Table S1, ESI.† Anal. calcd (%) for $C_{40}H_{48}V_2N_6O_8$: C, 57.01; H, 5.74 and N, 9.97; found: C, 57.37; H, 5.48 and N, 9.82. ESI-MS (p^+) (Fig. S9, ESI†) *m*/*z* for one asymmetric unit $C_{20}H_{24}VN_3O_4$ calculated: 421.37, found: 422.14; selected FTIR bands (KBr, cm^{-1}) (Fig. S10, ESI†): 3185 *ν*(O–H); 2970 *ν*(C–Har); 1244

 © 2023 The Author(s). Published by the Royal Society of Chemistry

Open Access Article. Published on 28 April 2023. Downloaded on 11/13/2025 1:50:14 PM.
This article is licensed under a Creative Commons Attribution-NonCommercial 3.0 Unported Licence.

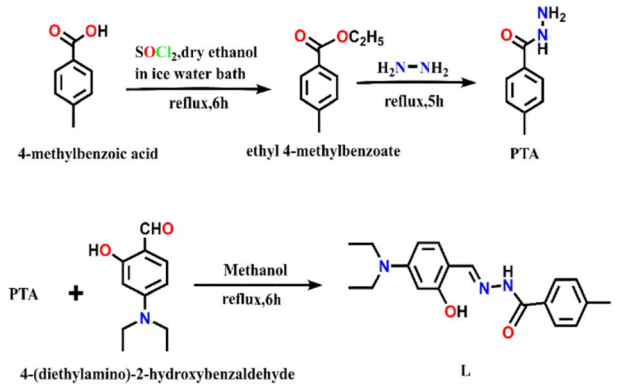

Scheme 1 Synthesis of PTA and L.

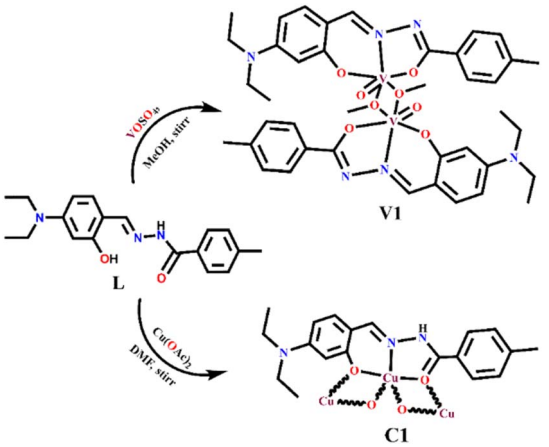

Scheme 2 Synthesis of V1 and C1.

ν(N–N); 1188 ν(C–O), stretching vibration; 963 ν(V=O); 830 ν [V–(μ-O)–V] mode and 1586 ν(C=N). The UV-vis spectrum in aqueous methanol (1 : 1, v/v, 10 μM, Fig. S11, ESI†): λ, nm (ε, M^{-1} cm^{-1}); 371 (37 000).

1D Cu(II) coordination polymer (C1). **C1** was prepared by mixing a solution of $Cu(OAc)_2$ (0.051 g, 1 mmol, and 5 mL) in DMF with a prestirred solution of **L** (0.091 g, 1 mmol, and 5 mL) in DMF. The stirring was continued for 3 hours, and the resulting intense green solution was used for slow evaporation. After 15 days, X-ray quality green crystals were collected at 81% yield and analysed by SC-XRD, as aforementioned. **C1** belongs to the '$P\bar{1}$' space group. The crystallographic refinement parameters are listed in Table S1, ESI.†

ESI-MS (p^+) (Fig. S12, ESI†) m/z calcd for $C_{19}H_{22}Cu_3N_3O_4$: 547.04, found: 547.99. FTIR (KBr, cm^{-1}): 3085 ν(N–H); 3370 ν(OH); 2970 ν(C–Har); 1601 ν(C=N) (Fig. S13, ESI†). UV-vis. spectrum in $CHCl_3$ solution λ_{max}/nm (ε_{max}/M^{-1} cm^{-1}): 395 (64 000), 415 (53 000) (Fig. S14, ESI†).

General procedure for catalytic studies

Oxidation of sulphide. A mixture of sulfide (5.0 mmol), catalyst (**V1**) (50 mg), and 30% hydrogen peroxide (10 mmol) was magnetically stirred in acetonitrile at room temperature

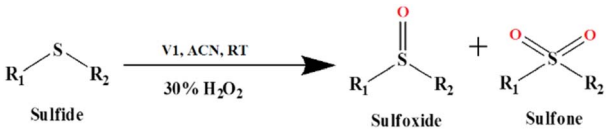

Scheme 3 The V1 catalyzed oxidation of sulfide.

(Scheme 3). After completion of the reaction, the catalyst was separated by filtration and washed with ethyl acetate. The product was extracted with ethyl acetate. The organic layer was dried over anhydrous Na_2SO_4. After the solvent was removed, the product was subjected to gas chromatographic (GC) analysis to determine its yield.

Aryl-sulphur cross-coupling using thiophenol and aryl iodide. To a mixture of iodobenzene (1 mmol) and thiophenol (1.1 mmol), 3 mL water, K_2CO_3 (276 mg) and **C1** (15 mg) were added. At the end of a specified time, the reaction mixture was filtered for analysis by GC and compared with standard references. The identification of the reaction products was performed by GC-MS analysis.

Results and discussion

Single crystal X-ray structures of L, V1 and C1

The ORTEP view of **V1** along with the atom labelling scheme is presented in Fig. 1a. A summary of the crystallographic data and refinement details for **L**, **V1** and **C1** is presented in Table S1 (ESI†). The **V1** belongs to the orthogonal crystal system with space group $P\bar{1}$. Each unit in the symmetric dinuclear vanadium(V) complex is coordinated by one nitrogen (N_2) and two oxygen (O_1 and O_2) donors of the ligand. One terminal oxo (O_4) donor is also present along with a methoxy group (O_3). The latter (O_3) acts as a μ^2-bridging unit to bind two identical parts of the complex together. Two square pyramidal asymmetric units form the complete structure of **V1**, where the central μ^2-bridging methoxy group imposes a V···V separation of ~3.337 Å, with a V–O–V bridging angle of ~107.30(12)° and O–V–O angles of 72.70(12)° (Fig. 1b). The methoxido groups display two different V–O distances, 1.853(3) Å and 2.278(3) Å. The former is quite longer than other reported oxovanadium(V) complexes[116] but similar to other bis-(μ-methoxy) bridged vanadium(V) dimer, 1.8207(13) Å.[117] Other V–O bonds are V–O_{oxide}, 1.597(3) Å, V–O_{ketone}, 1.955(3) Å and V–$O_{phenolate}$, 1.857(3) Å. The vanadium–oxygen bond lengths follow the order V–O_{oxido} < V–O_{alkoxo} < V–$O_{phenolate}$ < V–O_{ketone}. The V–N_{imine} bond length of 2.090(4) Å is comparable to the literature values.[118] Thus, **V1** is highly distorted, and vanadium centres deviate from the equatorial plane. The selected bond lengths and angles for **V1** are presented in Table S2 (ESI†).

The ORTEP view of **C1** is presented in Fig. 2a along with the atom labelling scheme. The **C1** crystallizes in triclinic space group $P\bar{1}$, while the asymmetric unit comprises the independent molecule [$C_{19}H_{21}CuN_3O_2$] where the Cu(II) centre is attached to imine nitrogen (N_2) and two oxygen (O_1 and O_2 from hydrazide and aldehyde moiety, respectively) atoms of the ligand. O_1 and O_2 act as end-on bridging groups and link [$C_{19}H_{21}CuN_3O_2$]

Open Access Article. Published on 28 April 2023. Downloaded on 11/13/2025 1:50:14 PM.
This article is licensed under a Creative Commons Attribution-NonCommercial 3.0 Unported Licence.

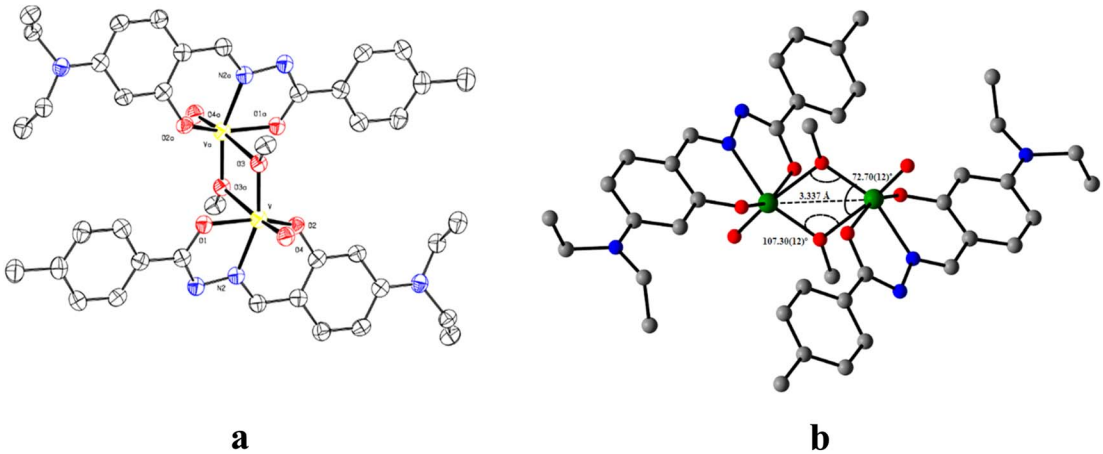

Fig. 1 (a) ORTEP of **V1** with 50% ellipsoid probability and (b) significant features around the bridging portion. H atoms are omitted for clarity.

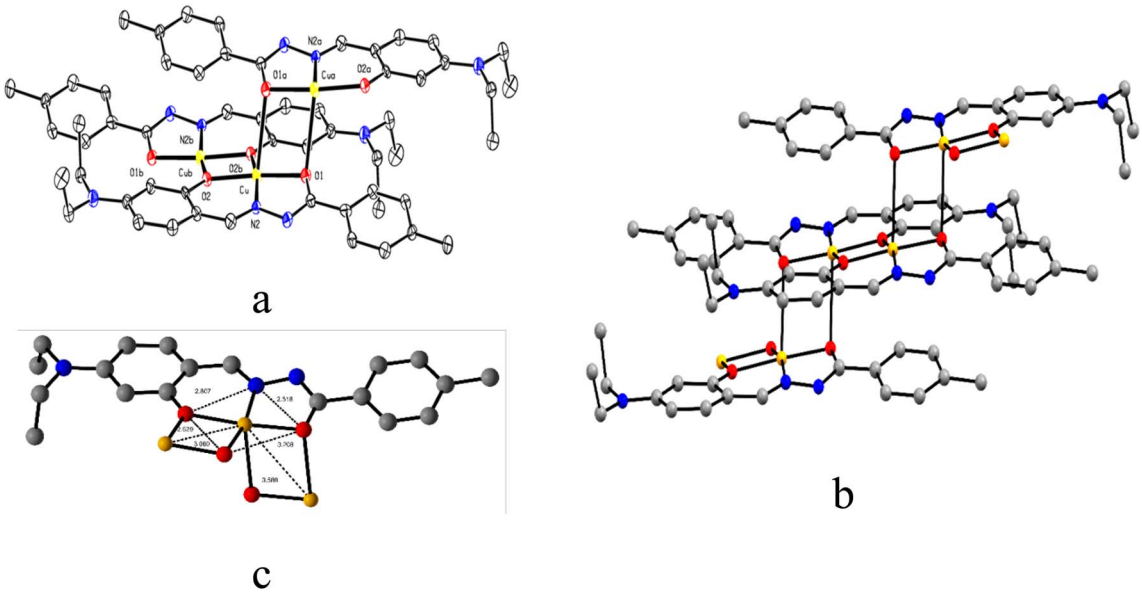

Fig. 2 (a) ORTEP view of **C1** with 50% ellipsoid probability, (b) 1D coordination polymer chain of **C1**, and (c) important distances around the central atom. H atoms are omitted for clarity.

moieties into a one-dimensional (1D) coordination polymer chain (Fig. 2b). The asymmetric unit $[C_{19}H_{21}CuN_3O_2]$ grows in a 1D polymer chain by two μ-oxo bridges having a bond angle of 86.96° with the other plane, resulting in two different Cu···Cu separations of ∼3.589 Å and 3.080 Å. In one identical unit, the Cu–O_1 distance is 1.982(5) Å, which differs from the other, Cu–O_2, 2.012(5) Å, while the Cu–N_2 distance is 1.896(5) Å, which varies in the 1D-polymer chain. In another plane, the distances are Cu–O_1, 2.675 Å and Cu–O_2, 1.972(4) Å. Significant distances around the central copper ion in one identical square plane are 3.203 Å, 2.807 Å, 2.529 Å and 2.518 Å (Fig. 2c). Important inter atomic distances and angles relevant to the copper(II) coordination sphere are presented in Table S3 (ESI†).

The ORTEP view along with the atom labelling scheme of **L** is presented in Fig. 3a. The **L** belongs to a triclinic crystal system with a $P\bar{1}$ space group. The molecules of **L** are self-assembled *via* a hydrogen bond between amide groups (N···O = 2.935 Å and angle N–N···O = 105.96°), leading to the formation of a 1D chain (Fig. 3b). Important bond distances and angles are presented in Table S4 (ESI†).

Fluorescence recognition of bilirubin using C1

To demonstrate the ability of **C1** to act as a bilirubin sensor, first, the media and their pH were optimized. Bilirubin is practically insoluble in water but soluble in bio-compatible organic solvent chloroform.[119] Therefore, to optimize solvent composition, several sets of solutions of **C1** and bilirubin have been prepared in chloroform/water (v/v), *viz.* 5 : 1, 4 : 1, 3 : 1, 2 : 1,1 : 1, 1 : 2, 1 : 3, 1 : 4 and 1 : 5 in PBS buffer at pH 8.0. It is observed that the solvent composition 1 : 4 (chloroform/water, v/v, PBS buffer, pH 8.0) is the best to monitor their interaction

 © 2023 The Author(s). Published by the Royal Society of Chemistry

Open Access Article. Published on 28 April 2023. Downloaded on 11/13/2025 1:50:14 PM.
This article is licensed under a Creative Commons Attribution-NonCommercial 3.0 Unported Licence.

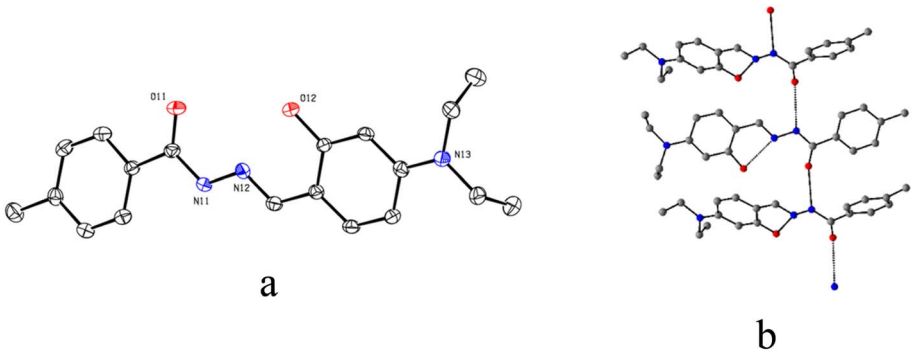

Fig. 3 (a) ORTEP view of **L** at 50% ellipsoid probability and (b) centro-symmetric disposition of three units self-assembled through hydrogen bond (black dashes). H atoms are omitted for clarity.

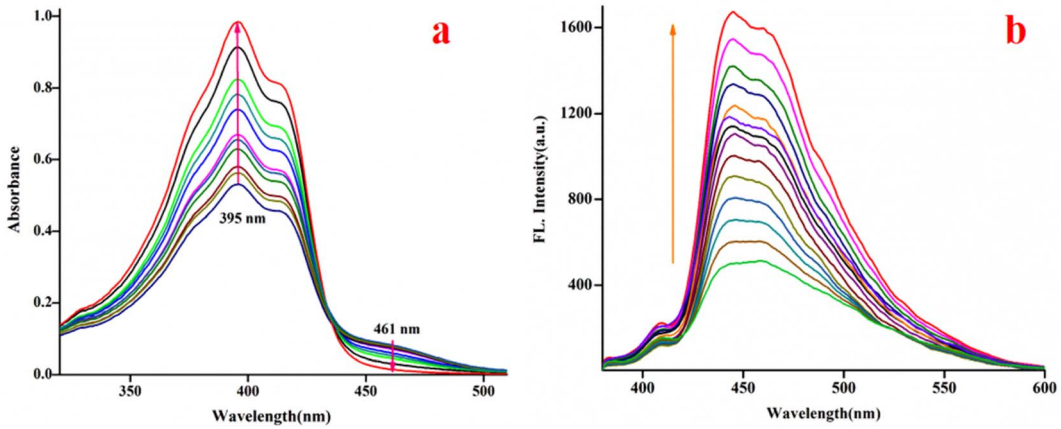

Fig. 4 Changes in the spectra of **C1** (20 μM, λ_{ex}, 369 nm, λ_{em}, 444 nm) upon the gradual addition of bilirubin (0–2500 μM, $CHCl_3$/water, 1/4, v/v, 0.1 M PBS buffer, pH 8.0), (a) absorption; (b) emission.

using spectroscopy (emission and absorption). The **C1** (20 μM) exhibits absorptions at 377 nm, 395 nm, 415 nm and 461 nm in the media, as stated earlier. Upon the gradual addition of bilirubin to **C1**, the shoulder at 461 nm further weakens markedly, whereas the absorbance at 395 nm increased gradually with an isobestic point at 434 nm (Fig. 4a), indicating their interaction.

The fluorescence experiments were performed in the same solvent system (chloroform/water, 1/4, v/v, PBS buffer, pH 8.0) at 25 °C. The **C1** (λ_{ex}, 369 nm) is weakly fluorescent owing to the quenching (*via* energy transfer and/or electron transfer from the excited state of fluorescence probe to a low-lying empty d-orbital of the Cu^{2+}) nature of paramagnetic Cu^{2+} ion (d^9-system).[120–122] The **C1** in solution alone (20 μM) exhibited weak emission at 444 nm and 460 nm with almost the same intensity. The incremental addition of bilirubin to **C1** (20 μM) resulted in significant fluorescence enhancement at both wavelengths (Fig. 4b). However, the emission band centred at 444 nm increased to a higher extent than the emission band at 460 nm. The fluorescence enhancement of **C1** in the presence of externally added bilirubin occurred because of the displacement of fluorescent amide-imine moiety (**L**, as an indicator) from the coordination sphere of **C1** (*via* IDA process[113,114]), or in other words, Cu^{2+} is extracted from **C1** by bilirubin to liberate free fluorescent **L**, resulting in fluorescence enhancement (Scheme 4).

This displacement event is also corroborated by Job's plot (Fig. S15†), mass spectrum (Fig. S16†) and FTIR spectrum (Fig. S17 and S18†) of the **C1**-bilirubin molecular assembly. In the mass spectrum of the **C1**-bilirubin molecular assembly, we found peaks at $m/z = 647.35$, 675.47, and 697.52 for the **C1** and $m/z = 370.30$ for the displaced **L** as indicators. Again, comparing the FTIR spectrum of the **C1**-bilirubin molecular assembly with the FTIR spectrum of pure bilirubin[123] and **C1**, we found distinctively different band positions and shapes of those spectra that indicate the formation of new adducts (Fig. S17 and S18†). The characteristics of IR stretching frequencies for free bilirubin and its adduct with **C1** are summarized in Table S5.†

However, fluorescence titration indicates that after the addition of a certain amount of bilirubin (2500 μM), the emission intensity remains almost unaltered (Fig. S19†). The displacement equilibrium constant is evaluated using Hill's equation:[124,125]

$$\log[Y/(1 - Y)] = n \log[G] + \log K,$$

Open Access Article. Published on 28 April 2023. Downloaded on 11/13/2025 1:50:14 PM.
This article is licensed under a Creative Commons Attribution-NonCommercial 3.0 Unported Licence.

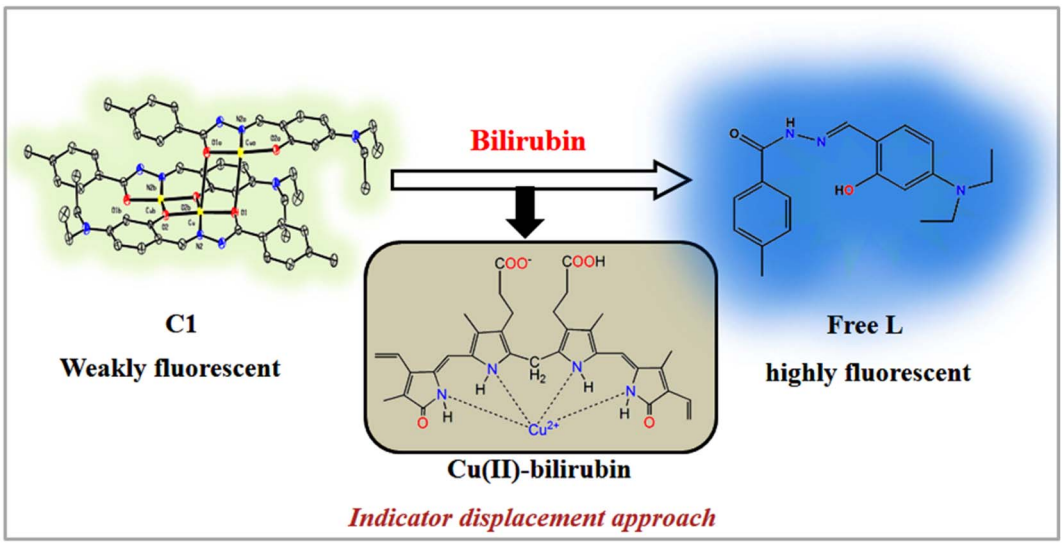

Scheme 4 Proposed bilirubin sensing mechanism of **C1**.

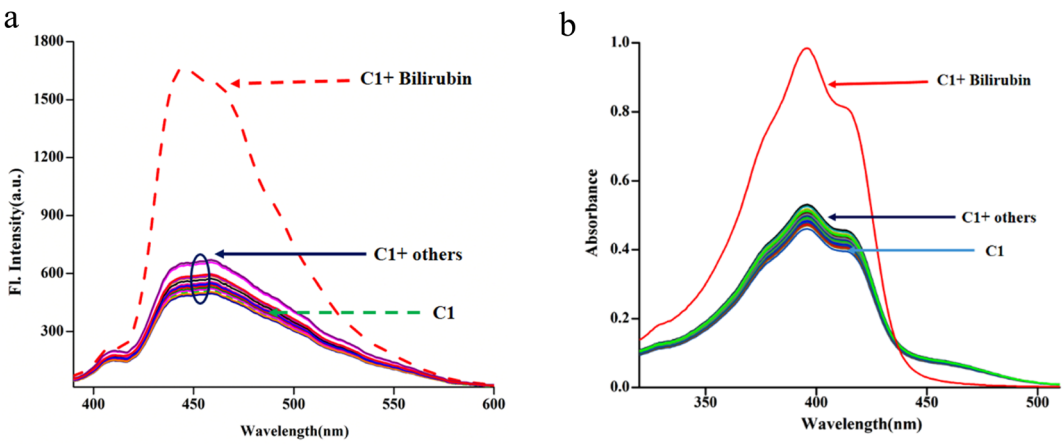

Fig. 5 Spectra of **C1** (20 μM, λ_{ex}, 369 nm) in the presence of amino acids, bio-relevant ions and biomolecules *viz.* Met, Arg, Cys, Pro, Lys, Trp, Phe, Gly, Asp, Na^+, K^+, Ca^{2+}, Mg^{2+} and Cyt C, SOD, bisphenol, insulin, creatinine, GSH, uric acid (100 μM; chloroform/water, 1/4, v/v, PBS buffer, pH, 8.0), (a): emission and (b): absorption.

Fig. 5 where Y, n, $[G]$ and K_{app} represent the fraction of ligand binding sites filled, Hill coefficient, and the concentration of guest (bilirubin) and displacement equilibrium constant, respectively. The value of the Hill coefficient describes the cooperativity of ligand binding in the following way: $n > 1$, positive cooperativity; $n = 1$, non-cooperativity and $n < 1$, negative cooperativity. Y is determined from the following equation: $Y = (F_x - F_0)/(F_{max} - F_x)$, where F_0, F_x, and F_{max} are emission intensities of **C1** in the absence of bilirubin, at intermediate bilirubin concentration, and at the concentration of complete interaction, respectively. The value of K is 7.78×10^5 M^{-1} (Fig. S20†). The detection limit for bilirubin, determined by $\frac{3\sigma}{K}$ method,[126] is 1.15 nM (Fig. S21†). We know that the development of sensors specific to any analyte in the complex background of potentially competing species is very challenging and requires extensive studies for any potential interferences. Hence, the effects of several bio-relevant ions *viz.* Na^+, K^+, Ca^{2+}, Mg^{2+}, α-amino acids *viz.* methionine, arginine, cysteine, proline, lysine, tryptophan, phenylalanine, glycine, aspartic acid and bio-molecules *viz.* cytochrome C, superoxide dismutase, bisphenol, insulin, creatinine, glutathione and uric acid are tested (Fig. 5a and b). No significant interferences are observed (Fig. S22†).

V1 catalyzed H_2O_2-assisted oxidation of sulphide

Oxidation of sulphide to sulfoxide and sulfone is important for the synthesis of several chemicals and pharmaceuticals. Hence, the catalytic activity of **V1** for the oxidation of sulphide in diphenyl sulphide using hydrogen peroxide (Scheme 5) is investigated as a model reaction.

To optimize reaction conditions, first, the effect of solvent (methanol, DMF, acetonitrile, $CHCl_3$ and toluene) and amount

 © 2023 The Author(s). Published by the Royal Society of Chemistry

Open Access Article. Published on 28 April 2023. Downloaded on 11/13/2025 1:50:14 PM.
This article is licensed under a Creative Commons Attribution-NonCommercial 3.0 Unported Licence.

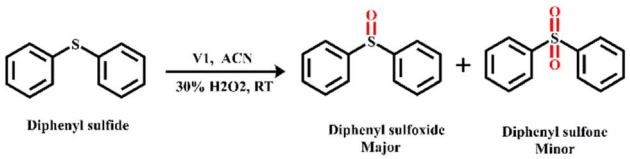

Scheme 5 H_2O_2-assisted oxidation of diphenyl sulphide using **V1** as a catalyst.

of H_2O_2 were tested (Table S5, ESI†). The highest yield of the product is observed in acetonitrile (Table S5, entry 3, ESI†). Protic solvents favour yield, whereas less polar solvents are very ineffective (Table S5, entries 4, 5, ESI†). Solvents, such as ethyl cyanide and iso-propanol, give low product yield (Table S6, entries 6, 7, ESI†).

At a low concentration of H_2O_2 (5 mmol), the yield of the product is low and requires a longer reaction time. The increasing amount of H_2O_2 from 5 mmol (Table S5,† entry 8) to 10 mmol (run 3) increases the product yield. However, a further increase to 15 mmol of H_2O_2 (Table S6,† entry 9) did not improve the yield but led to a higher amount of sulfone over sulfoxide.

To expand the scope of the conversion, oxidation reactions with several other sulphides (aliphatic and aromatic sulphides) were investigated and found to have a significantly high conversion rate and selectivity for sulfoxide under mild conditions (Table 1). It is interesting to note that the reaction rate becomes slow with the increased chain length of the alkyl group of the sulphide moiety. This may be due to the orientation of the hydrophobic alkyl chain around the sulphur centre. In addition, the reactivity and the conversion rate depend on the nature of the substituents present in the aryl moiety of ArSMe. The electron donating substituents accelerate the rate, whereas electron withdrawing substituents retard the rate (Table 1, entries 7 and 8). Interestingly, the yield of diphenyl sulfoxide is lower than

Table 1 The **V1** catalyzed oxidation of sulphide functionality using 30% H_2O_2[a]

Entry	Sulfide	Conversion (%)[b] (time, h)	Selectivity of sulfoxide[b] (%)
1	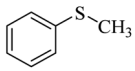	98 (3)	96
2	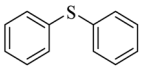	96 (3)	91
3	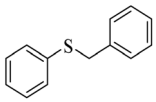	91 (5)	90
4	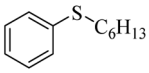	83 (6)	93
5	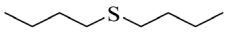	81 (4)	81
6	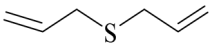	78 (4)	79
7	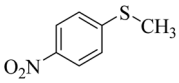	98 (3)	94
8	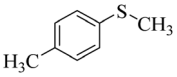	91 (3)	93
9	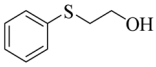	90 (5)	81
10	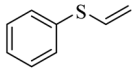	81 (5)	87
11	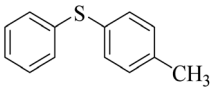	85 (5)	94
12[c]	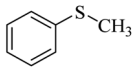	Trace	Trace

[a] Reaction conditions: sulphide (5 mmol); 30% aqueous H_2O_2 (10 mmol); CH_3CN (10 mL), RT; 50 mg catalyst. [b] Conversion and selectivity were determined using GC. [c] Without catalyst.

Open Access Article. Published on 28 April 2023. Downloaded on 11/13/2025 1:50:14 PM.
This article is licensed under a Creative Commons Attribution-NonCommercial 3.0 Unported Licence.

Table 2 The C–S cross-coupling reactions involving thiophenol and aryl iodide using **C1** as a catalyst[a]

Entry	ArI	Ar–SH	Products	Yield[b] (%)
1	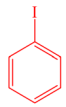		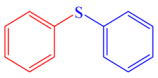	98
2	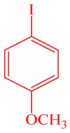	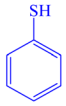	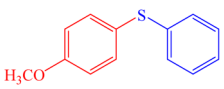	70
3		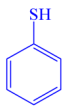	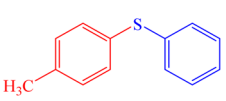	81
4		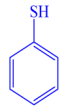	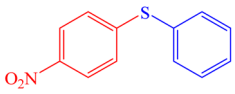	89
5	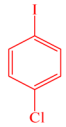	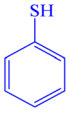	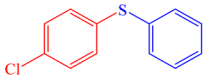	38
6	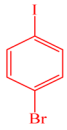	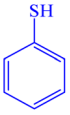	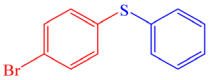	91
7	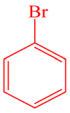	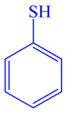	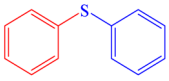	60
8	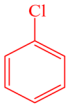	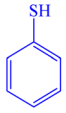	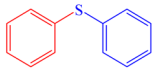	39
9	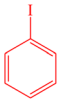	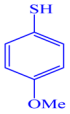	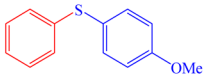	70
10[c]	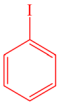	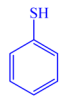	No reaction	No reaction

[a] Reaction conditions: aryl iodides (1 mmol), thiophenol (1.1 mmol), water (3 mL), K_2CO_3 (2 mmol) and **C1** (15 mg), temperature (90 °C), and time (12 h). [b] Yields were determined by GC analysis. [c] Without catalyst.

that of methyl phenyl sulfoxide probably due to the steric effect. The catalyst (**V1**) exhibited excellent chemo-selectivity towards the thio-centre over other oxidation prone functional groups, *viz.* C=C and OH (Table 2, entries 9 and 10).

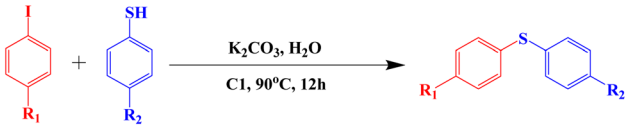

R_1 = H, CH_3, OCH_3, NO_2, Br, Cl; R_2 = H, OMe, Cl

Scheme 6 The C–S cross-coupling reaction of thiophenol with aryl iodide using **C1** as a catalyst.

Aryl-sulphur coupling of thiophenol with aryl iodide using C1 as a catalyst

The catalytic efficiency of **C1** for aryl-sulphur (C–S) cross-coupling in a model reaction involving thiophenol and aryl iodide to prepare diaryl sulphide is investigated (Scheme 6).

The effects of base and solvent are summarized in Table S7 (ESI†). Among different solvents that have been examined for the S-arylation reaction, *viz.* DMSO, DMF and H_2O, it is found that the yield is highest in water, ~98% (Table S7,† entry 3). The effect of the base is also investigated. Among various inorganic and organic bases tested, such as K_2CO_3, Et_3N, Cs_2CO_3 and KOH, it is found that the efficiency of KOH is poor, while that of Cs_2CO_3 is moderate and K_2CO_3 performs the best. Other bases are not effective at all (Table S7,† entry 3). It is interesting to note that the reaction does not proceed in the absence of any base (Table S7,† entry 6). Extreme moisture-sensitivity and cost of Cs_2CO_3 compelled us to choose more cheap and stable K_2CO_3 as the base for the C–S cross-coupling reaction.

To evaluate the scope and limitations and cover a broad range of aryl thiols and aryl iodides, the developed method is tested with substrates having different types of substituents. Under optimized conditions, as outlined in Table 2, the reactions are very clean and smooth with moderate yield. It is observed that aryl iodides with the electron withdrawing group were more reactive than those with the electron donating group. For example, aryl iodides containing methyl/methoxy group produced corresponding biphenyl derivatives in 70–81% yield (Table 2, entries 2 and 3). However, aryl iodides with nitro substituents produced the desired products with an 89% yield in water (Table 2, entry 4). The effect of halogen substituents on the C–S cross-coupling reactions involving thiophenol has the following reactivity order: iodobenzene > bromobenzene > chlorobenzene (Table 2).

Conclusion

Single crystal X-ray structurally characterized 1D copper(II) coordination polymer (**C1**) of an amide–imine conjugate (**L**), derived by condensation of 4-methyl-benzoic acid hydrazide (**PTA**) and 4-(diethylamino)-2-hydroxybenzaldehyde, efficiently recognizes bilirubin *via* 'turn-on' fluorescence through a ligand displacement approach. The displacement equilibrium constant is significantly high, 7.78×10^5 M^{-1}; the detection limit for bilirubin is 1.15 nM. The present method is superior to the available methods in terms of mechanism that imparts high selectivity, specificity and the lowest level of detection. Almost

 © 2023 The Author(s). Published by the Royal Society of Chemistry

Open Access Article. Published on 28 April 2023. Downloaded on 11/13/2025 1:50:14 PM.
This article is licensed under a Creative Commons Attribution-NonCommercial 3.0 Unported Licence.

all the reported probes are of unimpressive, undesirable "turn-off" kind. The only one of the "turn on" kind has LOD that is much higher than our present probe. According to the literature, the present probe has the lowest LOD for bilirubin (Table S8†). In addition, **C1** acts as a potential green catalyst for the C–S cross-coupling reaction in water. A dimeric oxo–vanadium complex (**V1**) of the **L** functions as a promising catalyst for the oxidation of sulphide. The structures of both **V1** and **L** were confirmed by SC-XRD analysis.

Conflicts of interest

There are no disagreement to mention.

Acknowledgements

We thank USIC, BU for extending SC-XRD facility.

References

1 G. Arthur, *The Amide Linkage: Selected Structural Aspects in Chemistry, Biochemistry, and Materials Science*, Wiley-Interscience, 2000.
2 J. M. Humphrey and A. R. Chamberlin, *Chem. Rev.*, 1997, **97**, 2243–2266.
3 X. Liu, L. Lin and X. Feng, *Chem. Commun.*, 2009, 6145–6158.
4 V. R. Pattabiraman and J. W. Bode, *Nature*, 2011, **480**, 471–479.
5 R. C. Larock, *Comprehensive Organic Transformation*, VCH, New York, 1999, 102.
6 S. Roy, S. Roy and G. W. Gribble, *Tetrahedron*, 2012, **68**, 9867–9923.
7 J. Lee, S. K. Muthaiah and S. H. Hong, *Adv. Synth. Catal.*, 2014, **356**, 2653–2660.
8 S. C. Ghosh, J. S. Y. Ngiam, A. M. Seayad, D. T. Tuan, C. L. L. Chai and A. J. Chen, *J. Org. Chem.*, 2012, **77**, 8007–8015.
9 R. Cadoni, A. Porcheddu, G. Giacomelli and D. L. Luca, *Org. Lett.*, 2012, **14**, 5014–5017.
10 D. M. Flanigan, F. Romanov-Michailidis, N. A. White and T. Rovis, *Chem. Rev.*, 2015, **115**, 9307–9387.
11 P. Noblia, M. Vieites, B. S. Parajo n-Costa, E. J. Baran, H. Cerecetto, P. Draper, M. Gonzalez, O. E. Piro, E. E. Castellano, A. Azqueta, D. L. Cerain A, A. Monge-Vega and D. Gambino, *J. Inorg. Biochem.*, 2005, **99**, 443–451.
12 Y. Shechter, I. Goldwaser, M. Mironchik, M. Fridkin and D. Gefel, *Coord. Chem. Rev.*, 2003, **237**, 3–11.
13 A. M. B. Bastos, J. G. da Silva, P. I. S. Maia, V. M. Deflon, A. A. Batista, A. V. M. Ferreira, L. M. Botion, E. Niquet and H. Beraldo, *Polyhedron*, 2008, **27**, 1787–1794.
14 S. Naskar, M. Corbella, A. J. Blake and S. K. Chattopadhyay, *Dalton Trans.*, 2007, **11**, 1150–1159.
15 L. Reytman, O. Braitbard, J. Hochman and E. Y. Tshuva, *Inorg. Chem.*, 2016, **55**, 610–618.
16 K. K. Bedia, O. Elçin, U. Seda, K. Fatma, S. Nathaly, R. A. Sevim and A. Dimoglo, *Eur. J. Med. Chem.*, 2006, **41**, 1253–1261.
17 P. Melnyk, V. Leroux, C. Sergheraert, P. Grellier and C. Sergheraert, *Bioorg. Med. Chem. Lett.*, 2006, **16**, 31–35.
18 R. R. Eady, *Coord. Chem. Rev.*, 2003, **237**, 23–30.
19 A. Butler and J. V. Walker, *Chem. Rev.*, 1993, **93**, 1937–1944.
20 K. H. Thompson, J. H. McNeill and C. Orvig, *Chem. Rev.*, 1999, **99**, 2561–2572.
21 M. Nikoorazm, A. Ghorbani-Choghamarani and N. Noori, *Appl. Organometal. Chem.*, 2015, **29**, 328–333.
22 M. C. Carreno, *Chem. Rev.*, 1995, **95**, 1717–1760.
23 X. F. Wu, *Tetrahedron Lett.*, 2012, **53**, 4328–4331.
24 V. Conte, F. Di Furia and G. Licini, *Appl. Catal., A*, 1997, **157**, 335–361.
25 B. Li, A. H. Liu, L. N. He, Z. Z. Yang, J. Gao and K. H. Chen, *Green Chem.*, 2012, **14**, 130–135.
26 H. J. Kim and J. S. Kim, *Tetrahedron Lett.*, 2006, **47**, 7051–7055.
27 M. Hirano, S. Yakabe, J. H. Clark and T. Morimoto, *J. Chem. Soc., Perkin Trans. 1*, 1996, **1**, 2693–2698.
28 A. Rostami, B. Tahmasbi, F. Abedi and Z. Shokri, *J. Mol. Catal. A: Chem.*, 2013, **378**, 200–205.
29 A. M. henkin, G. Leitus and R. Neumann, *J. Am. Chem. Soc.*, 2010, **132**, 11446–11448.
30 J. Gao, H. Guo, S. Liu and M. Wang, *Tetrahedron Lett.*, 2007, **48**, 8453–8455.
31 R. Das and D. Chakraborty, *Tetrahedron Lett.*, 2010, **51**, 6255–6258.
32 R. Das and D. Chakraborty, *Synthesis*, 2011, **2**, 277–280.
33 D. Chakraborty, P. Malik and V. K. Goda, *Appl. Organomet. Chem.*, 2012, **26**, 21–26.
34 P. Malik and D. Chakraborty, *Tetrahedron Lett.*, 2012, **53**, 5652–5655.
35 R. Fazaeli, H. Aliyan, S. P. Foroushani, Z. Mohagheghian and Z. Heidari, *Iran J. Catal.*, 2013, **3**, 129–137.
36 F. Lebon, N. Boggetto, M. Ledecq, F. Durant, Z. Benatallah, S. Sicsic and M. Reboud-Ravaux, *Biochem. Pharmacol.*, 2002, **63**, 1863.
37 B. Kumari, S. Kundu, K. Ghosh, M. Banerjee, S. K. Pradhan, S. M. Islam, P. Brandao, V. Felix and D. Das, *Dalton Trans.*, 2018, **47**, 14008.
38 Y. Zhou, J. Won, J. Y. Lee and J. Yoon, *Chem. Commun.*, 2011, **47**, 1997.
39 Z. Li, X. Lou, Z. Li and J. A. Qin, *ACS Appl. Mater. Interfaces*, 2009, **2**, 232.
40 Y. Zhou and J. Yoon, *Chem. Soc. Rev.*, 2012, **41**, 52.
41 I. P. Beletskaya and V. P. Ananikov, *Chem. Rev.*, 2011, **111**, 1596–1636.
42 A. Gangjee, Y. Zeng, T. Talreja, J. J. McGuire, R. L. Kisliuk and S. F. Queener, *J. Med. Chem.*, 2007, **50**, 3046–3053.
43 I. P. Beletskaya and A. V. Cheprakov, Copper in cross-coupling reactions: the post-Ullmann chemistry, *Coord. Chem. Rev.*, 2004, **248**, 2337–2364.
44 S. Di Bella and I. Fragala, *New J. Chem.*, 2002, **26**, 285–290.
45 G. De Martino, M. C. Edler, G. La Regina, A. Cosuccia, M. C. Barbera, D. Barrow, R. I. Nicholson, G. Chiosis,

Open Access Article. Published on 28 April 2023. Downloaded on 11/13/2025 1:50:14 PM.
This article is licensed under a Creative Commons Attribution-NonCommercial 3.0 Unported Licence.

A. Brancale, E. Hamel, M. Artico and R. Silvestri, *J. Med. Chem.*, 2006, **49**, 947–954.
46 A. Jabbari, H. Mahdavi, M. Nikoorazm and A. Ghorbani-Choghamarani, *J. Porous Mater.*, 2015, **22**, 1111–1118.
47 G. Y. Li, *Angew. Chem., Int. Ed.*, 2001, **40**, 1513–1516.
48 M. Murata and S. L. Buchwald, *Tetrahedron*, 2004, **60**, 7397–7403.
49 M. A. Fernández-Rodríguez, Q. Shen and J. F. Hartwig, *Chem.–Eur. J.*, 2006, **12**, 7782–7796.
50 T. Itoh and T. Mase, *Org. Lett.*, 2004, **6**, 4587–4590.
51 Y. Zhang, K. N. Ngeow and J. Y. Ying, *Org. Lett.*, 2007, **9**, 3495–3498.
52 S. Jammi, P. Barua, L. Rout, P. Saha and T. Punniyamurthy, *Tetrahedron Lett.*, 2008, **49**, 1484–1487.
53 Y. C. Wong, T. T. Jayanth and C. H. Cheng, *Org. Lett.*, 2006, **8**, 5613–5616.
54 V. P. Reddy, K. Swapna, A. V. Kumar and K. R. Rao, *J. Org. Chem.*, 2009, **74**, 3189–3191.
55 A. Correa, M. Carril and C. Bolm, *Angew. Chem., Int. Ed.*, 2008, **47**, 2880–2883.
56 W. Y. Wu, J. C. Wang and F. Y. Tsai, *Green Chem.*, 2009, **11**, 326–329.
57 J. She, Z. Jiang and Y. G. Wang, *Tetrahedron Lett.*, 2009, **50**, 593–596.
58 F. Y. Kwong and S. L. Buchwald, *Org. Lett.*, 2002, **4**, 3517–3520.
59 C. G. Bates, P. Saejueng, M. Q. Doherty and D. Venkataraman, *Org. Lett.*, 2004, **6**, 5005–5008.
60 Y. J. Chen and H. H. Chen, *Org. Lett.*, 2006, **8**, 5609–5612.
61 M. S. Kabir, M. Lorenz, M. L. Van-Linn, O. A. Namjoshi, S. Ara and J. M. Cook, *J. Org.Chem.*, 2010, **75**, 3626–3643.
62 R. Xu, J. Wan, H. Mao and Y. Pan, *J. Am. Chem. Soc.*, 2010, **132**, 15531–15533.
63 F. Luo, C. Pan, L. Li, F. Chen and J. Cheng, *Chem. Commun.*, 2011, **47**, 5304–5306.
64 D. K. Dumbrea, P. R. Selvakannana, S. K. Patil, V. R. Choudhary and S. K. Bhargava, *Appl. Catal., A*, 2014, **476**, 54–60.
65 S. Khanra, S. Ta, A. Paladhi, M. Ghosh, S. Ghosh, S. K. Hira, P. P. Manna, P. Brandão, V. Félix and D. Das, *Chem. Commun.*, 2020, **56**, 6563–6566.
66 D. L. Ma, V. P. Y. Ma, D. S. H. Chan, K. H. Leung, H. Z. He and C. H. Leung, *Coord. Chem. Rev.*, 2012, **256**, 3087–3113.
67 L. You, D. Zha and E. V. Anslyn, *Chem. Rev.*, 2015, **115**(15), 7840–7892.
68 D. L. Ma, W. L. Wong, W. H. Chung, F. Y. Chan, P. K. So, T. S. Lai, Z. Y. Zhou, Y. C. Leung and K. Y. Wong, *Angew. Chem., Int. Ed.*, 2008, **47**, 3735–3739.
69 Y. Zhou and J. Yoon, *Chem. Soc. Rev.*, 2012, **41**, 52–67.
70 M. Bonizzoni, L. Fabbrizzi, G. Piovani and A. Taglietti, *Tetrahedron*, 2004, **60**, 11159–11162.
71 G. Klein and J. L. Reymond, *Angew. Chem.*, 2001, **113**, 1821–1823.
72 H. Aït-Haddou, S. L. Wiskur, V. M. Lynch and E. V. Anslyn, *J. Am. Chem. Soc.*, 2001.
73 S. Das, A. Banerjee, S. Lohar, B. Sarkar, S. K. Mukhopadhyay, J. S. Matalobos, A. Sahana and D. Das, *New J. Chem.*, 2014, **38**, 2744–2747.
74 P. A. Zunszain, J. Ghuman, A. F. McDonagh and S. Curry, *J. Mol. Biol.*, 2008, **381**, 394–406.
75 K. Abha, J. Nebu, J. S. A. Devi, R. S. Aparna, R. R. Anjana, A. O. Aswathy and S. George, *Sens. Actutors, B*, 2019, **282**, 300–308.
76 P. Novotna, F. Kralik and M. Urbanova, *Biophys. Chem.*, 2015, **205**, 41–50.
77 M. Martelanc, L. Ziberna, S. Passamonti and M. Franko, *Talanta*, 2016, **154**, 92–98.
78 B. Batra, S. Lata, J. S. Rana and C. Shekhar, *Biosens. Bioelectron.*, 2013, **44**, 64–69.
79 L. Ngashangva, V. Bachu and P. Goswami, *J. Pharm. Biomed. Anal.*, 2019, **162**, 272–285.
80 X. P. Li and Z. Rosenzweig, *J. Anal. Chim. Acta*, 1997, **353**, 263–273.
81 S. S. Tikmani, H. J. Warraich, F. Abbasi, A. G. Rizvi, L. Darmstadt and A. K. Zaidi, *Trop. Med. Int. Health*, 2010, **15**, 502–507.
82 S. Sherlock and J. Dooley, *Diseases of the Liver and Biliary System*, Blackwell Science Ltd, 2007, pp. 205–218.
83 S. C. Kazmierczak, A. F. Robertson, P. G. Catrou, B. L. Briley and G. R. Gourley, *Clin. Chem.*, 2002, **48**, 1096–1097.
84 A. Sevillanocabeza, M. C. Alberolagarbi and P. Campinsfalco, *Microchem. J.*, 1994, **50**, 14–27.
85 J. Zelenka, M. Lenícek, L. Muchová, M. Jirsa, M. Kudla, P. Balaz, M. Zadinová, J. D. Ostrow, R. J. Wong and L. Vítek, *J. Chromatogr. B*, 2008, **867**, 37–42.
86 S. Itoh, K. Isobe and S. Onishi, *J. Chromatogr. A*, 1999, **848**, 169–177.
87 C. Lu, J. M. Lin and C. W. Huie, *Talanta*, 2004, **63**, 333–337.
88 H. S. Lee, M. M. Karim, S. M. Alam and S. H. Lee, *Luminescence*, 2007, **22**, 331–337.
89 J. W. Liu, X. M. Zhou and M. G. Zhang, *Chin. J. Chromatogr.*, 1998, **16**, 369.
90 Z. Nie and Y. S. Fung, *Electrophoresis*, 2008, **29**, 1924–1931.
91 K. Kurosaka, S. Senba, H. Tsubota and H. Kondo, *Clin. Chim. Acta*, 1998, **269**, 125–136.
92 A. Kosaka, C. Yamamoto, Y. Morishita and K. Nakane, *Clin. Biochem.*, 1987, **20**, 451–458.
93 V. Amendola, L. Fabbrizzi, F. Forti, M. Licchelli, C. Mangano, P. Pallavicini, A. Poggi, D. Sacchi and A. Taglieti, *Coord. Chem. Rev.*, 2006, **250**, 273–299.
94 K. Rurack and U. Resch-Genger, *Chem. Soc. Rev.*, 2002, **31**, 116–127.
95 S. Das, M. Dutta and D. Das, *Anal. Methods*, 2013, **5**, 6262–6285.
96 T. Senthilkumar and S. K. Asha, *Macromolecules*, 2015, **48**, 3449–3461.
97 Y. Du, X. Li, X. Lv and Q. Jia, *ACS Appl. Mater. Interfaces*, 2017, **9**, 30925–30932.
98 C. Xia, Y. Xu, M. M. Cao, Y. P. Liu, J. F. Xia, D. Y. Jiang, G. H. Zhou, R. J. Xie, D. F. Zhang and H. L. Li, *Talanta*, 2020, **212**, 120795.

 © 2023 The Author(s). Published by the Royal Society of Chemistry

Open Access Article. Published on 28 April 2023. Downloaded on 11/13/2025 1:50:14 PM.
This article is licensed under a Creative Commons Attribution-NonCommercial 3.0 Unported Licence.

99 M. Santosh, S. R. Chinnadayyala, A. Kakoti and P. Goswami, *Biosens. Bioelectron.*, 2014, **59**, 370–376.
100 S. K. Anand, M. R. Mathew and K. G. Kumar, *J. Fluoresc.*, 2019, **30**, 63–70.
101 M. Jayasree, R. S. Aparna, R. R. Anjana, J. S. A. Devi, N. John, K. Abha, A. Manikandan and S. George, *Anal. Chim. Acta*, 2018, **1031**, 152–160.
102 S. Ellairaja, K. Shenbagavalli, S. Ponmariappan and V. S. Vasantha, *Biosens. Bioelectron.*, 2017, **91**, 82–88.
103 S. M. Babin and R. M. Sova, *Anal. Chem. Insights*, 2014, **9**, 59–64.
104 S. M. Wabaidur, G. E. Eldesoky and Z. A. Alothman, *Luminescence*, 2018, **33**, 625–629.
105 R. R. Anjana, J. S. A. Devi and M. Jayasree, *Microchim. Acta*, 2018, **185**, 11.
106 Y. Wei, F. X. Jin, H. Z. Guo and Y. J. Dan, *Anal. Bioanal. Chem.*, 2018, **410**, 6459–6468.
107 V. Srinivasan, M. A. Jhonsi, N. Dhenadhayalan, K. C. Lin, D. A. Ananth, T. Sivasudha, R. Narayanaswamy and A. Kathiravan, *Spectrochim. Acta, Part A*, 2019, **221**, 117150.
108 S. K. Makkad and S. K. Asha, *ACS Appl. Polym. Mater.*, 2019, **1**, 1230–1239.
109 M. Zhang, L. Xu, Q. Ma, H. Yu, H. Fang, Z. Lin, Q. Zhang and Z. Chen, *ACS Appl. Mater. Interfaces*, 2018, **10**, 42155–42166.
110 W. Bian, N. Zhang and C. Jiang, *Luminescence*, 2011, **26**, 54–58.
111 W. Bian, N. Zhang and L. Wang, *Anal. Sci.*, 2010, **26**, 785–789.
112 B. T. Nguyen and E. V. Anslyn, *Coord. Chem. Rev.*, 2006, **250**, 3118–3127.
113 S. Das, S. Guha, A. Banerjee, S. Lohar, A. Sahana and D. Das, *Org. Biomol. Chem.*, 2011, **9**, 7097–7104.
114 S. Ta, M. Ghosh, K. Ghosh, P. Brandão, V. Félix, S. K. Hira, P. P. Manna and D. Das, *ACS Appl. Bio Mater.*, 2019, **2**, 2802–2811.
115 B. Mondal, M. G. Drew and T. Ghosh, *Inorg. Chim. Acta*, 2009, **362**, 3303–3308.
116 E. Seena, N. Mathew, M. Kuriakose and M. P. Kurup, *Polyhedron*, 2008, **27**, 1455–1462.
117 H. H. Monfared, R. Bikas, P. M. Anarjan, A. J. Blake, V. Lippolis, N. B. Arslan and C. Kazak, *Polyhedron*, 2014, **69**, 90–102.
118 R. Brodersen, *J. Biol. Chem.*, 1979, **254**, 2364–2369.
119 Y. Q. Weng, F. Yue, Y. R. Zhong and B. H. Ye, *Inorg. Chem.*, 2007, **46**, 7749–7755.
120 O. Sahin and M. Yilmaz, *Tetrahedron*, 2011, **67**, 3501–3508.
121 L. J. Tang and M. J. Cai, *Sens. Actuators, B*, 2012, **173**, 862–867.
122 M. Maity, S. Das and N. C. Maiti, *Phys. Chem. Chem. Phys.*, 2014, **16**, 20013–20022.
123 S. Shinkai, M. Ikeda, A. Sugasaki and M. Takeuchi, *Acc. Chem. Res.*, 2001, **34**, 494–503.
124 M. Ghosh, S. Ta, J. S. Matalobos and D. Das, *Dalton Trans.*, 2018, **47**, 11084–11090.
125 A. Ghorai, J. Mondal, R. Chandra and G. K. Patra, *Dalton Trans.*, 2015, **44**, 13261–13271.
126 M. Ghosh, S. Ta, S. Lohar, S. Das, P. Brando, V. Felix and D. Das, *J. Mol. Recognit.*, 2018, **32**, 2771–2778.